MINISTRY OF INDUSTRY AND TRADE
**HANOI UNIVERSITY OF INDUSRY**

**----------**

**TRUONG CONG DOANH**

# SYNTHESIS OF ZINC BORATE, ALUMINUM HYDROXIDE AND HYDROTALCITE IN NANO-PLATE FORM FOR APPLICATION IN THE FABRICATION OF FLAME-RETARDANT POLYMER COMPOSITES

Major: Chemical Engineering

Code: 9520301

**SUMMARY OF DISSERTATION IN CHEMICAL ENGINEERING**

Hanoi, 2025

This desertation has been completed at:

**HANOI UNIVERSITY OF INDUSRY**

**Scientific supervisors:**

**1. Assoc. Prof. Dr. Hoang Mai Ha**

**2. Assoc. Prof. Dr. Vu Minh Tan**

**Reviewer 1: Assoc. Prof. Dr. Nguyen Phuong Hoai Nam**

**Reviewer 2: Assoc. Prof. Dr. Nguyen Thanh Tung**

**Reviewer 3:Assoc. Prof. Dr. Dam Xuan Thang**

The desertation was defended at the Doctoral Evaluating Council at University level, held at Hanoi University of Industry at …., date….. 2026

The desertation can be found at**:**

- The library of Hanoi University of Industry
- Vietnam National Library

# INTRODUCTION

## 1. Reason for choosing the topic

Nowadays, polymer materials are widely used in various fields of daily life and industry due to their advantages such as low density, high mechanical strength, chemical stability, corrosion resistance, and ease of processing and shaping. However, the major drawback of polymers is their flammability, resulting from their chemical structure and organic composition, which significantly limits their applications in sectors requiring high fire safety, such as electronics, construction, automotive, textiles, and aerospace. Therefore, improving the fire resistance of polymer materials is of both scientific and practical significance.

Two main approaches are applied to slow down or prevent polymer combustion: (i) directly introducing flame-retardant functional groups into the polymer structure through chemical reactions; and (ii) incorporating flame-retardant additives to produce polymer composites. The first approach provides long-lasting effectiveness but is difficult and costly to implement. The second approach is more convenient and cost-effective, though its efficiency and mechanical performance strongly depend on the type and amount of additives.

Organic additives generally offer good flame-retardant performance but often contain halogens, which release dense smoke and toxic gases upon combustion, posing risks to health and the environment. In contrast, inorganic additives are safer, cheaper, and capable of smoke suppression, but they usually require high loadings, leading to particle agglomeration, poor dispersion, and deterioration of mechanical properties. To overcome these limitations, current research focuses on developing inorganic flame retardants at the nanoscale and modifying their surfaces with organic agents to enhance dispersion and compatibility with polymer matrices. This strategy not only improves flame-retardant efficiency but also reduces additive loading, thereby maintaining or enhancing the mechanical properties of the material.

Based on the above reasons, I chose the research direction *"Synthesis of zinc borate, aluminum hydroxide, and hydrotalcite in nano-plate form for application in the fabrication of flame-retardant polymer composites"*, aiming to contribute to the practical development of polymer materials that combine excellent mechanical performance with enhanced fire safety.

## 2. Research purpose

This study aims to synthesize several inorganic, nano-structured materials in thin-plate form, including nano zinc borate (nZB), nano aluminum hydroxide (nATH), and nano hydrotalcite (nHT), with controlled morphology and structure. Their surfaces are to be modified or organically hybridized to improve dispersion in polymer matrices, serving as additives for developing flame-retardant composites based on polypropylene (PP) and epoxy (EP) resins.

## 3. Research content

- Study on the synthesis and determination of morphology, structure, and properties of nZB.
- Study on the synthesis and determination of morphology, structure, and properties of nATH.

- Study on the synthesis and determination of morphology, structure, and properties of nHT.

- Study on the fabrication of flame-retardant nanocomposites based on thermoplastic PP using the synthesized nanoparticles as additives.

- Study on the fabrication of flame-retardant nanocomposites based on thermosetting EP resins using the synthesized nanoparticles as additives.

**4. Research Methodology**

- Synthesis of nano-structured materials.

- Fabrication of flame-retardant composite materials.

- Investigation and characterization of the morphology and properties of nano-structured materials.

- Evaluation of the properties of flame-retardant materials.

**5. Scientific and practical significance of the dissertation**

The dissertation clarifies the synthesis, structural characteristics, and optimized morphology of inorganic nano-materials such as ZB, ATH, and HT. It expands the understanding of the relationship between structure, morphology, and flame-retardant performance, and reveals a strong synergistic effect when combining these nanoparticles with different flame retardants in PP and EP matrices. The flame-retardant mechanisms were found to occur simultaneously in both gas and condensed phases, contributing to the scientific basis of halogen-free polymer composites.

The developed materials show excellent flame-retardant performance, with epoxy-based composites achieving UL-94 V-0 rating and LOI values above 30%, while polypropylene-based systems also exhibit improved fire resistance and mechanical properties with reduced additive content, leading to better cost efficiency. The use of halogen-free, environmentally friendly additives aligns with sustainable development trends and demonstrates strong potential for industrial application in advanced flame-retardant polymer composites.

**6. Structure of the dissertation**

Besides the Introduction, the dissertation is organized into three chapters followed by the Conclusions and Recommendations:

Chapter 1. Overview

Chapter 2. Experimental work and research methodology

Chapter 3. Results and discussion

Conclusions and recommendations.

## CHAPTER 1 – OVERVIEW

This chapter provides an overview of previous studies in Vietnam and abroad related to the following topics:

**1.1. Overview of the combustion mechanisms of polymer materials and the flame-retardant mechanisms of additives, including a review of currently used flame retardants**

**1.2. Overview of nano-structured flame-retardant materials**

**1.3. Overview of research on the preparation of flame-retardant polymer nanocomposites based on polypropylene and epoxy resins**

# CHAPTER 2 – EXPERIMENTAL WORK AND RESEARCH METHODOLOGY

## 2.1. Chemicals, equipment, and experimental instruments

## 2.2. Methods for material synthesis and fabrication

### *2.2.1. Synthesis of inorganic nano-plate materials*

*2.2.1.1. Synthesis of nano zinc borate*

Nano-structured ZB was synthesized via a precipitation method from a homogeneous solution [145]. In this process, $Na_2B_4O_7.10H_2O$ and oleic acid were first dissolved, followed by the dropwise addition of a $ZnSO_4.7H_2O$ solution into the mixture at 70 $^oC$ under continuous stirring for 6.5 hours. The resulting precipitate was filtered, washed sequentially with ethanol and distilled water, and then dried at 80 $^oC$ for 12 hours to obtain nZB.

*2.2.1.2. Synthesis of nano aluminum hydroxide*

Nano ATH was synthesized via a hydrothermal method from $Al(NO_3)_3.9H_2O$. Aluminum nitrate was dissolved in distilled water and subsequently reacted with 1 M NaOH solution under controlled pH (≈5) to form a precursor gel. The gel was centrifuged, thoroughly washed, and redispersed in 1 M NaOH solution at pH ≈ 9. The resulting suspension was subjected to hydrothermal treatment in a Teflon-lined autoclave at various temperatures and reaction times. The obtained white solid was collected by centrifugation, repeatedly washed with distilled water, and dried at 80 $^oC$ for 12 h to obtain nATH.

*2.2.1.3. Synthesis of nano hydrotalcite*

Nano HT was synthesized as follows: Solution (1) containing $Mg(NO_3)_2.6H_2O$ and $Al(NO_3)_3.9H_2O$ with molar ratios Mg/Al = 1.5, 2.0, 2.5, and 3.0, and solution (2) containing NaOH and $Na_2CO_3$ with $Al/CO_3^{2-}$ = 1.33, were simultaneously added dropwise into 500 mL of distilled water in a 2000 mL beaker under continuous magnetic stirring (500 rpm) at 65 $^oC$, maintaining the pH = 8 - 10. After addition, the mixture was further stirred at 65 $^oC$ for 2 hours. The resulting white suspension was aged under various conditions, followed by filtration, repeated washing, and drying at 70 $^oC$ for 24 hours to obtain nHT.

### *2.2.2. Modification of nanostructured materials*

*2.2.2.1. Surface modification of nano aluminum hydroxide*

The surface of nATH was modified using one of the following organic agents: oleic acid (OA), Tween 80 (Tw80), or polyethylenimine (PEI). The modifying agents (3 wt% relative to nATH) were dissolved in a specific amount of ethanol. The nATH powder was then added to the solution, and the mixture was continuously stirred at 60 $^oC$ for 2 hours. Ethanol was subsequently removed by rotary evaporation under reduced pressure, and the obtained products were denoted as $nATH_{OA}$, $nATH_{Tw80}$, and $nATH_{PEI}$, respectively.

*2.2.2.2. Modification of nano hydrotalcite with an organophosphorus flame-retardant agent*

Nano HT was modified with 9,10-dihydro-9-oxa-10-phosphaphenanthrene-10-oxide (DOPO) at mass ratios of 1:1, 2:1, 3:1, and 4:1 (DOPO:HT). DOPO was dissolved in ethanol to form a homogeneous solution, into which HT was dispersed. The mixture was refluxed at 90 $^oC$ with vigorous stirring for 4 hours, then the solvent was removed by rotary evaporation. The obtained solid was

ground into a fine white powder and designated as $HT_1$, $HT_2$, $HT_3$, and $HT_4$, corresponding to the respective mass ratios.

***2.2.3. Preparation of fire-resistant polymer composites***

*2.2.3.1. Preparation of fire-resistant polymer composites based on PP*

Fire-resistant PP nanocomposites were prepared using nZB as a flame-retardant additive. PP and the additives were dried at 80 $^oC$ for 12 h, then melt-blended in a Haake Rheomix 610 mixer (Germany) at 175 $^oC$, 50 rpm for 8 min. The melt was compression-molded into sheets (150 × 150 × 3.2 mm) using a Toyoseiki hydraulic press (Japan) at 200 $^oC$ and 10-12 MPa for 4 min. The samples were cooled, conditioned for 24 h, and cut to standard sizes for mechanical and flame-resistance tests.

*2.2.3.2. Preparation of fire-resistant polymer composites based on EP*

*+ Modification of ammonium polyphosphate with polyethyleneimine*

Ammonium polyphosphate (APP) was modified with PEI via a cation-exchange reaction [129]. Solvent A was prepared by mixing 210 mL of absolute ethanol and 10 mL of distilled water. PEI (3.5 g) was dissolved in 20 mL of solvent A under nitrogen, while APP (10 g) was dispersed in the remaining 200 mL, heated to 90 $^oC$, and stirred vigorously under $N_2$. The PEI solution was then rapidly added to the APP dispersion, and the reaction continued at 90 °C for 2 h under an inert atmosphere. The solid product was filtered, washed repeatedly with ethanol, and vacuum-dried at 80 $^oC$ for 24 h to obtain APP@PEI powder.

*+ Preparation of fire-resistant epoxy-based polymer composites using nATH*

Epoxy nanocomposites were prepared via a conventional curing process with a hardener-to-resin mass ratio of 34:100, as recommended by the supplier (LR385). The flame retardants, including nATH and other additives, were dispersed in the hardener by mechanical stirring at 200 rpm for 15 min, followed by ultrasonication for 10 min. EP resin was then added and gently stirred at 100 rpm for 10 min until a homogeneous mixture was obtained. The mixture was poured into silicone molds of standard dimensions, cured at room temperature for 24 h, and post-cured at 60 °C for 12 h to complete the reaction.

*+ Preparation of fire-resistant epoxy-based polymer composites using nHT*

Epoxy nanocomposites containing nHT were prepared following the same procedure as for the epoxy nanocomposites containing nATH.

**2.3. Methods for characterizing morphology, structure, and properties of materials**

***2.3.1. Methods for investigating morphology and structure***

*2.3.1.1. Fourier transform infrared spectroscopy (FT-IR)*

FT-IR spectroscopy was employed to identify characteristic functional groups in the structures of nanomaterials. Measurements were conducted at the Pharmaceutical Chemistry Laboratory, Institute of Chemistry, Vietnam Academy of Science and Technology.

*2.3.1.2. X-Ray diffraction (XRD)*

XRD, a non-destructive method, was used to obtain structural information and crystal size of the materials. Analyses were performed at the Analytical Laboratory, Institute of Chemistry, Vietnam Academy of Science and Technology.

*2.3.1.3. Scanning electron nicroscopy (SEM)*

The surface morphology of nanostructured materials was examined using field emission scanning electron microscopy (FE-SEM) on a Hitachi S-4800 system at the Institute of Materials Science, Vietnam Academy of Science and Technology.

***2.3.2. Methods for investigating material properties***

*2.3.2.1. Determination of nanomaterial dispersion in polymer matrix*

The dispersion of nATH particles before and after surface functionalization in the polymer matrix was observed using an Eclipse Ts2 inverted optical microscope (Nikon, Japan).

*2.3.2.2. Evaluation of nanomaterial dispersion by EDX-mapping*

Elemental distribution of C, O, N, Al, and P in the nanocomposites was analyzed by energy-dispersive X-ray spectroscopy (EDX) using the Hitachi S-4800 SEM at the Institute of Materials Science, Vietnam Academy of Science and Technology.

*2.3.2.3. Thermogravimetric analysis (TGA)*

Thermal properties of inorganic nanomaterials and polymer nanocomposites were studied using a LABSYS Evo STA (Setaram, France) thermal analyzer at the Faculty of Chemistry, Hanoi University of Science, Vietnam National University.

*2.3.2.4. Limiting oxygen index (LOI) measurement*

The LOI of samples was determined using a Yasuda No.214 instrument (Japan) at the Key Laboratory of Polymer and Composite Materials, Hanoi University of Science and Technology.

*2.3.2.5. Vertical burning test (UL94-V)*

UL94-V testing was conducted to assess the flame retardancy of materials under vertical flame exposure according to ASTM D3801, using a GT-MC35F-2 apparatus (Gester, China) at the Functional Polymer and Nanomaterials Laboratory, Institute of Chemistry, Vietnam Academy of Science and Technology.

*2.3.2.6. Mechanical property measurements*

Tensile strength and elongation at break of the composites were measured using an AI-7000M tester (Gotech, Taiwan) at the Functional Polymer and Nanomaterials Laboratory, Institute of Chemistry, Vietnam Academy of Science and Technology.

Unnotched Izod impact strength was determined according to ASTM D4812 on a mechanical testing device (TestResources, USA) at the Tropical Engineering Institute (now Institute of Materials Science), Vietnam Academy of Science and Technology.

All mechanical measurements were performed at least five times, and the reported value represents the average of five measurements with the corresponding error.

*2.3.2.7. Characterization of char morphology in composites*

The surface morphology of char residues from burned composite samples was observed by FE-SEM (Hitachi S-4800, Japan) at an accelerating voltage of 5 kV. Energy-dispersive X-ray spectroscopy (EDX) was used to determine the elemental composition of the residues. Measurements were carried out at the Institute of Materials Science, Vietnam Academy of Science and Technology.

# CHAPTER 3 – RESULTS AND DISCUSSION

## 3.1. Results of synthesizing inorganic nanoparticles as fire-retardant additives

### *3.1.1. Morphology, structure, and properties of zinc borate nanomaterials*

*3.1.1.1. Morphology and structure of synthesized zinc borate nanoparticles*

*+ Morphology of synthesized nano zinc borate particles*

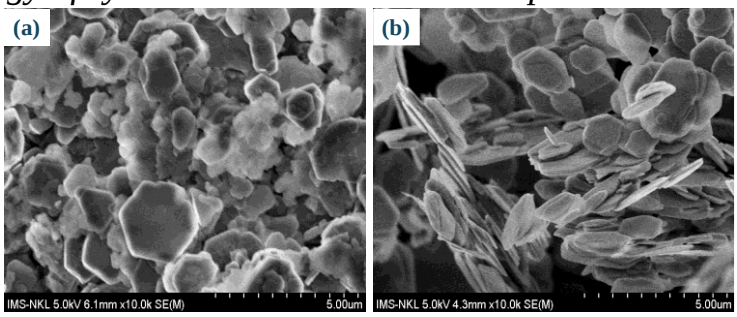


Figure 3.1. SEM images of nZB particles without (a) and with (b) oleic acid

Under the reaction conditions of 70 °C and the reaction time as described, the sample without surfactant for ZB nanoparticles obtained showed a polyhedral shape with a wide size distribution (0.5–2.5 μm), whereas the sample with OA yielded more uniform nanosheets (diameter 1.0–1.5 μm, thickness ~90 nm) (figure 3.1).

*+ The structure of synthesized nano zinc borate particles*

The structural characteristics of the synthesized ZB nanoparticles were investigated by FT-IR spectroscopy and XRD analysis. The results indicated that the obtained ZB nanoparticles are crystalline with the molecular formula $2ZnO.3B_2O_3.3H_2O$, exhibiting high purity, and in the sample synthesized with surfactant, the OA molecules were adsorbed on the particle surface.

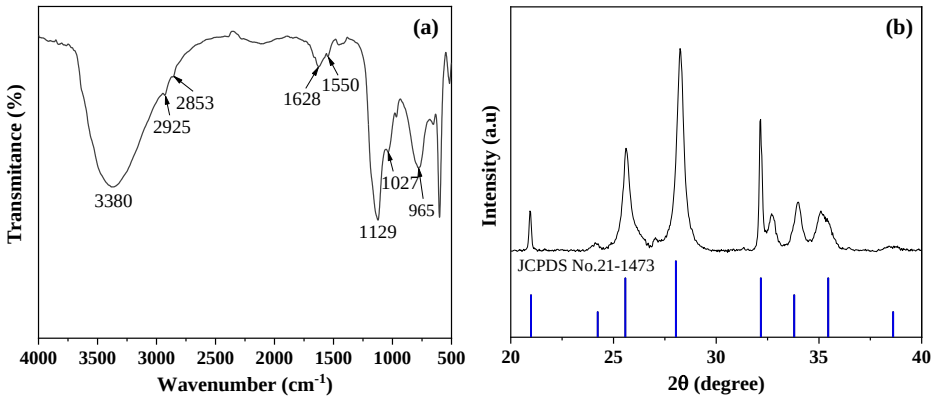


Figure 3.2. FT-IR spectrum (a) and XRD pattern (b) of nZB

*3.1.1.2. Thermal properties of zinc borate nanoparticles*

To verify that the synthesized product is zinc borate with the molecular formula $2ZnO.3B_2O_3.3H_2O$, the thermal properties were investigated using thermogravimetric analysis (TGA).

Thermal analysis (Figure 3.3) revealed that the zinc borate sample decomposed in the temperature range of 285–600 °C, with the most significant weight loss occurring at 420 °C. The total weight loss was 12.42%, attributed to the release of crystalline water, which is consistent with the molecular formula $2ZnO.3B_2O_3.3H_2O$.

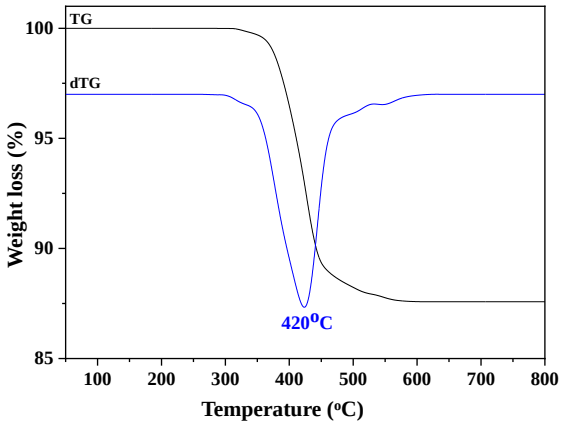


Figure 3.3. TG and DTG curves of nZB

*3.1.1.3. Hydrophobicity of zinc borate nanoparticles*

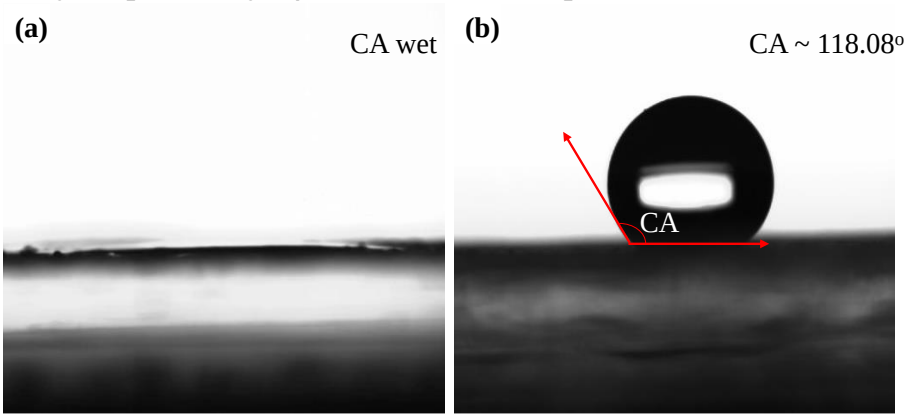


Figure 3.4. Water droplet contact angle images on the surfaces of nZB particles without (a) and with oleic acid (b)

The hydrophobicity of solid surfaces is commonly evaluated by water contact angle measurement. Results indicated that pristine ZB nanoparticles are superhydrophilic (contact angle ≈ 0°) and exhibit poor dispersion in polymers. However, upon surface modification with 3% oleic acid, the contact angle increased to ~118°, demonstrating a transition to hydrophobic behavior.

***3.1.2. Morphology, structure, and properties of aluminum hydroxide nanomaterials***

*3.1.2.1. Morphology and structural characteristics of synthesized aluminum hydroxide nanoparticles*

The synthesis conditions for nATH were investigated, and the results are summarized in Table 3.1.

Table 3.1. Synthesis conditions of ATH nanoparticles and the characteristics of the obtained products

| No. | Samples | Temp. (°C) | Time (h) | Product | Morphology | Yield (%) |
|---|---|---|---|---|---|---|
| 1 | nATH-1 | 80 | 72 | 77.7% gibbsite, 22.3% bayerite | Polygonal nanoplates | 75.6 |
| 2 | nATH-2 | 90 | 72 | Gibbsite | Hexagonal nanoplates | 82.5 |
| 3 | nATH-3 | 100 | 72 | Gibbsite | Hexagonal nanoplates | 80.8 |
| 4 | nATH-4 | 90 | 24 | Amorphous gel with minor gibbsite | Amorphous with minor hexagonal nanoplates | 8.2 |
| 5 | nATH-5 | 90 | 48 | Gibbsite | Hexagonal nanoplates | 32.3 |

Under the optimized synthesis conditions of hydrothermal temperature at 90 °C and reaction time of 72 h, the obtained ATH nanoparticles exhibited a hexagonal plate-like morphology with a diameter of 200–300 nm and a thickness of approximately 50 nm. The particles were predominantly in the gibbsite phase, making them suitable for the fabrication of flame-retardant nanocomposites.

*3.1.2.2. Thermal properties of aluminum hydroxide nanoparticles*

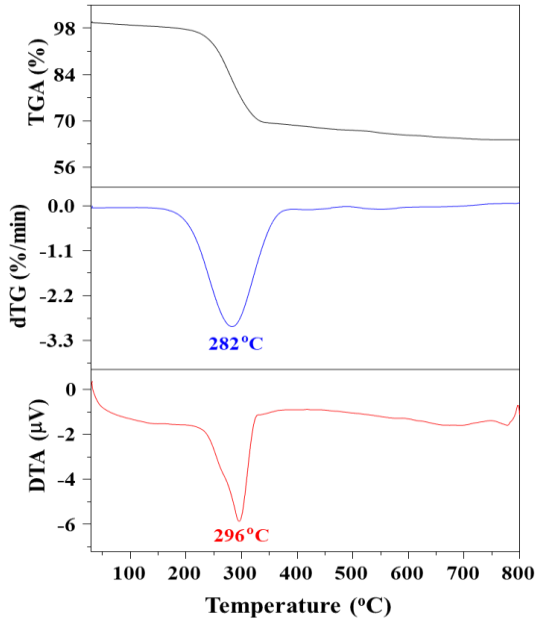


Figure 3.9. TGA, DTG, and DTA curves of nATH

The thermal properties of ATH nanoparticles were investigated using thermogravimetric analysis (TGA). Figure 3.9 presents the TG, DTG, and DTA curves of the ATH nanoparticle sample. Figure 3.9 shows that the ATH nanoparticle sample exhibited a slight weight loss below 180 °C due to the evaporation of adsorbed water. The main decomposition stage occurred between 180 - 380 °C, with an endothermic peak at 296 °C corresponding to the transformation of aluminum hydroxide into $Al_2O_3$. The total weight loss reached 35.73%, which is consistent with the theoretical value.

*3.1.2.3. Surface modification of aluminum hydroxide nanoparticles with organic agents*

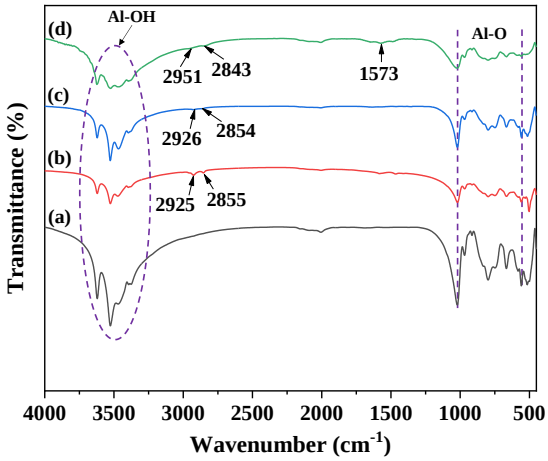


Figure 3.10. FT-IR spectra of nATH before and after modification with organic compounds: (a) nATH, (b) $nATH_{OA}$, (c) $nATH_{Tw80}$, and (d) $nATH_{PEI}$

To improve compatibility with the polymer matrix, the surface of nATH was modified with oleic acid, Tween 80, and polyethyleneimine, yielding the samples $nATH_{OA}$, $nATH_{Tw80}$, and $nATH_{PEI}$. The effectiveness of surface coverage was confirmed by FT-IR spectra (Figure 3.10).

Microscopic observations (Figure 3.11) revealed that $nATH_{PEI}$ exhibited the best dispersion in the epoxy matrix, with clearly separated nanoplatelets. The elemental mapping of Al in the nanocomposites further demonstrated that the PEI coating facilitated a more uniform distribution of $nATH_{PEI}$ in the $3nATH_{PEI}$/7IFR/EP sample compared with the unmodified nATH in the 3nATH/7IFR/EP sample.

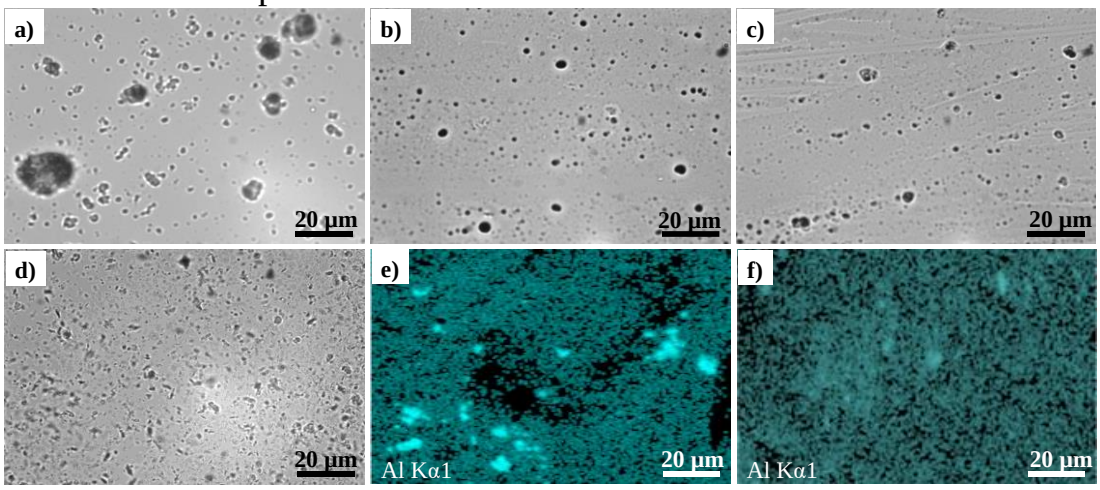


Figure 3.11. Optical micrographs showing the dispersion of nATH particles in the EP resin matrix before and after surface modification: nATH (a), $nATH_{OA}$ (b), $nATH_{Tw80}$ (c), and $nATH_{PEI}$ (d); and elemental Al distribution maps of the nanocomposite samples 3nATH/7IFR/EP (e) and $3nATH_{PEI}$/7IFR/EP (f)

### *3.1.3. Morphology, structure, and properties of hydrotalcit nanomaterials*

*3.1.3.1. Morphology and structure of synthesized hydrotalcite nanoparticles*

*+ Effect of the Mg/Al ratio on the morphology and structure of hydrotalcite nanoparticles*

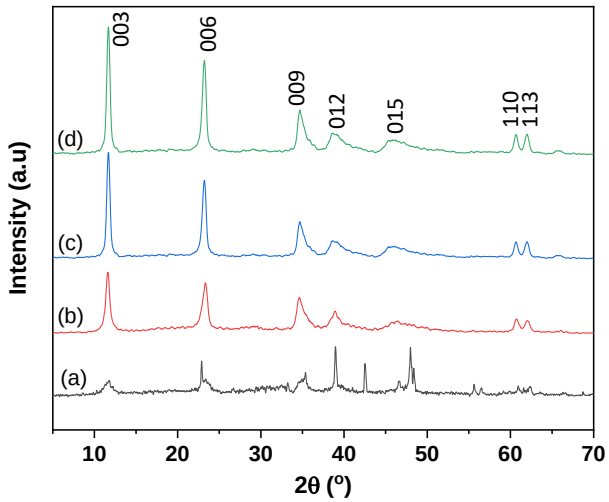


Figure 3.12. XRD patterns of nHT samples obtained at different Mg/Al molar ratios: (a) 1.5; (b) 2.0; (c) 2.5; and (d) 3.0

The effect of the Mg/Al molar ratio on the structure and morphology of hydrotalcite nanoparticles was evaluated by XRD (Figure 3.12) and SEM (Figure

3.13). The results indicated that the Mg/Al ratio of 2.5 was the most suitable for synthesizing HT nanoparticles, as the product exhibited a well-defined crystalline structure with sharp diffraction peaks and a uniform hexagonal platelet morphology, with a diameter of ~100 nm and a thickness of ~20 nm.

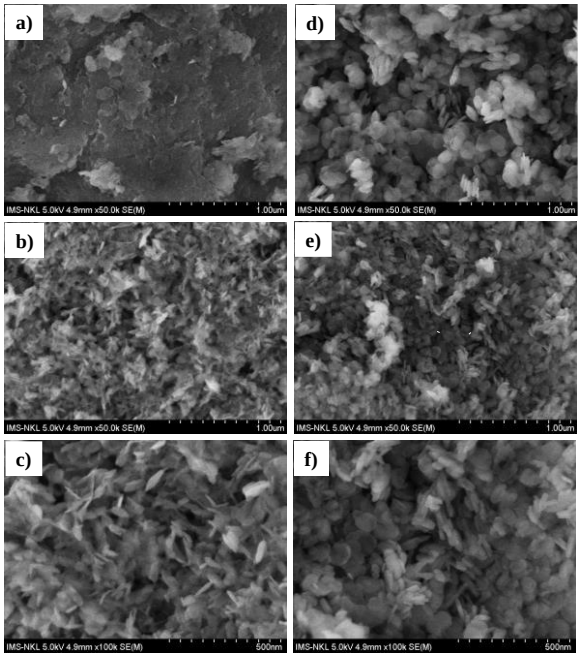


Figure 3.13. SEM images of nHT samples obtained at different Mg/Al molar ratios: (a) 1,5; (b, c) 2,0; (d) 2,5; and (e, f) = 3,0

*+ Effect of aging time and temperature on the morphology and structure of hydrotalcite nanoparticles*

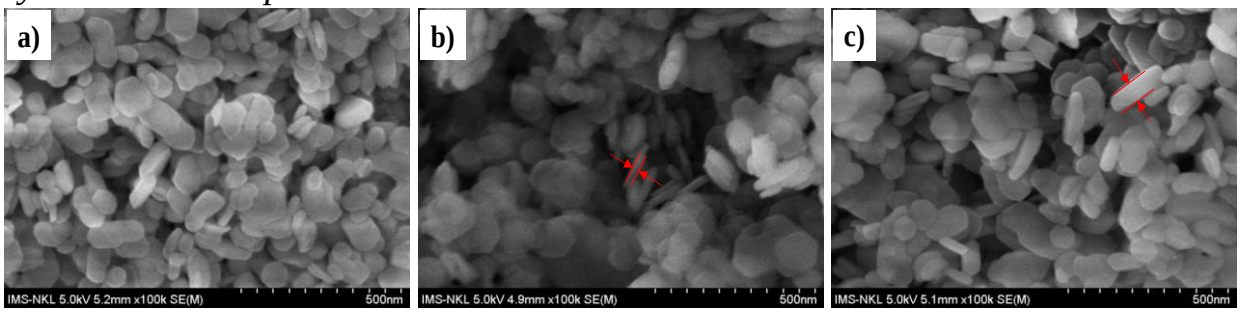


Figure 3.14. SEM images of nHT samples obtained at different aging times: (a) 14 h, (b) 24 h, and (c) 36 h

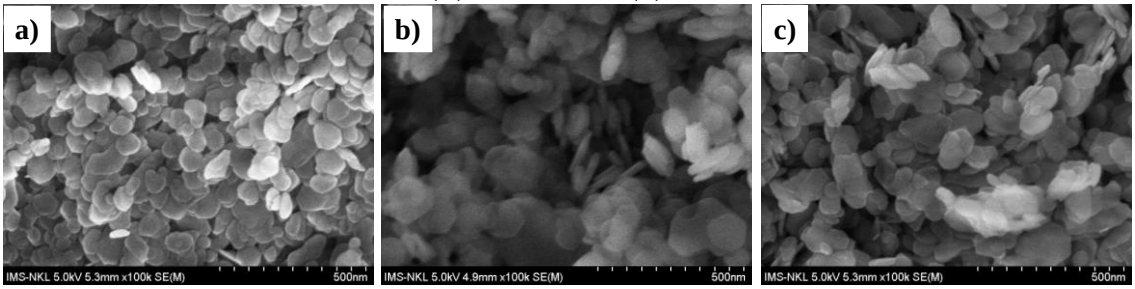


Figure 3.15. SEM images of HT samples obtained at different aging temperatures: (a) 80 °C, (b) 90 °C, and (c) 100 °C

SEM images (Figures 3.14 and 3.15) demonstrate that aging time and temperature have a significant influence on the morphology of hydrotalcite nanoparticles. After 14 h, the particles were irregular; after 24 h, uniform hexagonal platelets with a diameter of ~140–150 nm and a thickness of ~20 nm

were observed; and after 36 h, the crystallites became thicker (~45 nm). At 80 °C, the particles were small (~80 nm in diameter) with poorly defined structures; at 90 °C, well-defined and uniform hexagonal platelets were formed; whereas at 100 °C, the particles became irregular with large aggregates. Therefore, the optimal synthesis condition was determined to be 24 h of aging at 90 °C.

*3.1.3.2. Thermal properties of hydrotalcite nanoparticles*

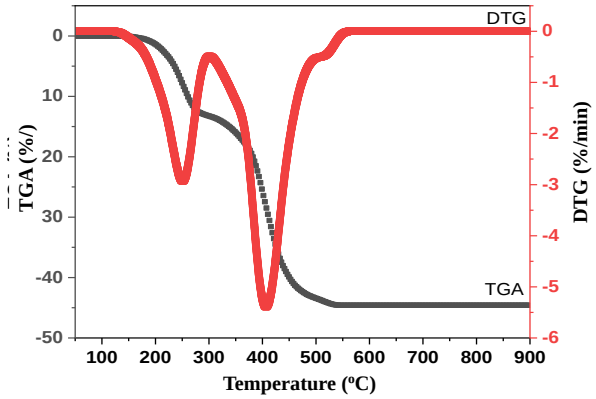


Figure 3.16. TGA and DTG curves of nHT.

The thermal properties of HT synthesized at an Mg/Al molar ratio of 2.5, with aging at 90 °C for 24 h, were analyzed by thermogravimetric analysis (TGA) (Figure 3.16). The results showed that HT underwent two stages of weight loss: the first stage (130–300 °C) with ~13.31% loss, attributed to the removal of surface and interlayer water; and the second stage (300–560 °C) with ~31.26% loss, corresponding to the decomposition of hydroxides and interlayer $CO_3^{2-}$ anions, leading to the formation of mixed metal oxides.

*3.1.3.3. Study on the modification of hydrotalcite nanoparticles using organophosphorus flame-retardant agents*

*+ Morphology and structure of hydrotalcite nanoparticles after surface modification*

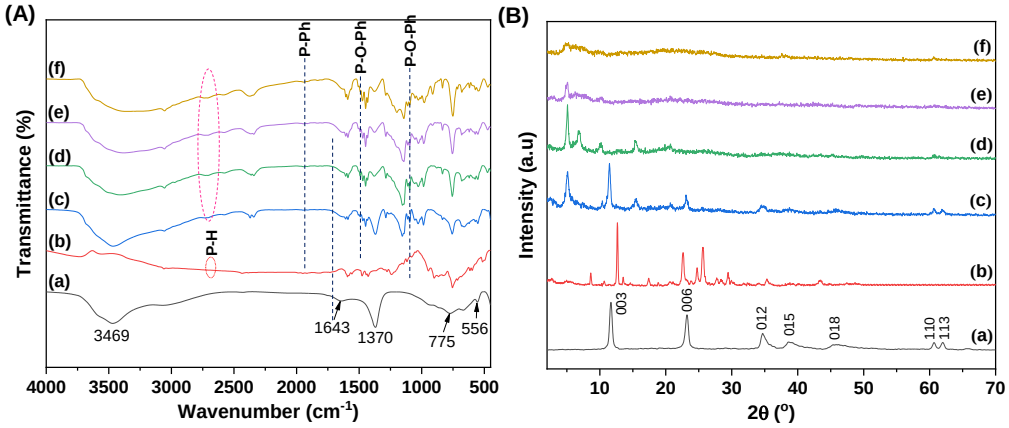


Figure 3.18. FT-IR spectra (A) and XRD patterns (B) of the samples: nHT (a), DOPO (b), $HT_1$ (DOPO:HT = 1:1) (c), $HT_2$ (DOPO:HT = 2:1) (d), $HT_3$ (DOPO:HT = 3:1) (e), and $HT_4$ (DOPO:HT = 4:1) (f)

FT-IR and XRD results indicated that DOPO molecules were intercalated between the hydrotalcite layers, replacing the interlayer water and forming hydrogen bonds with the hydroxyl groups of HT. As the DOPO content increased, the HT structure became more disordered, which favored layer exfoliation in the polymer matrix. Meanwhile, the SEM images (Figure 3.19) demonstrated a

pronounced morphological change, showing DOPO either coating or completely intercalating into the nHT particles, resulting in increased thickness and obscuring the original hexagonal plate-like shape.

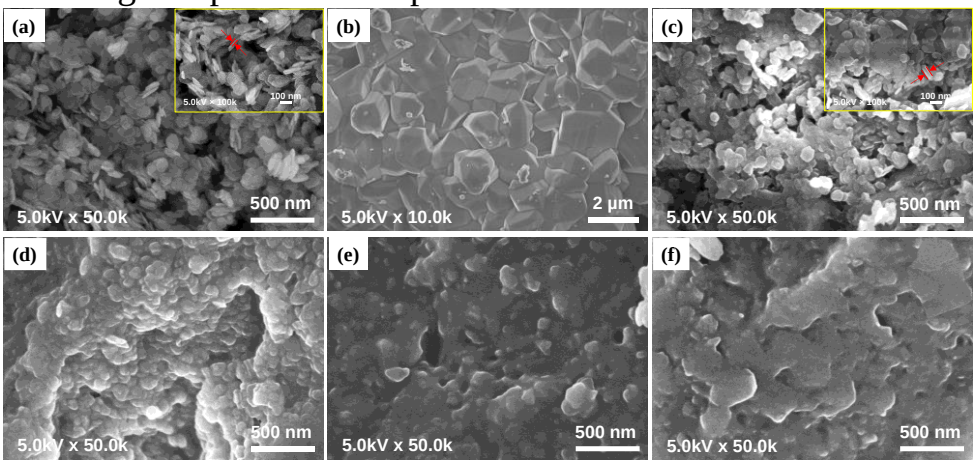


Figure 3.19. SEM images of the samples: nHT (a and inset), DOPO (b), $HT_1$ (DOPO:HT = 1:1) (c and inset), $HT_2$ (DOPO:HT = 2:1) (d), $HT_3$ (DOPO:HT = 3:1) (e), and $HT_4$ (DOPO:HT = 4:1) (f)

*+ Thermal properties of hydrotalcite nanoparticles after modification*

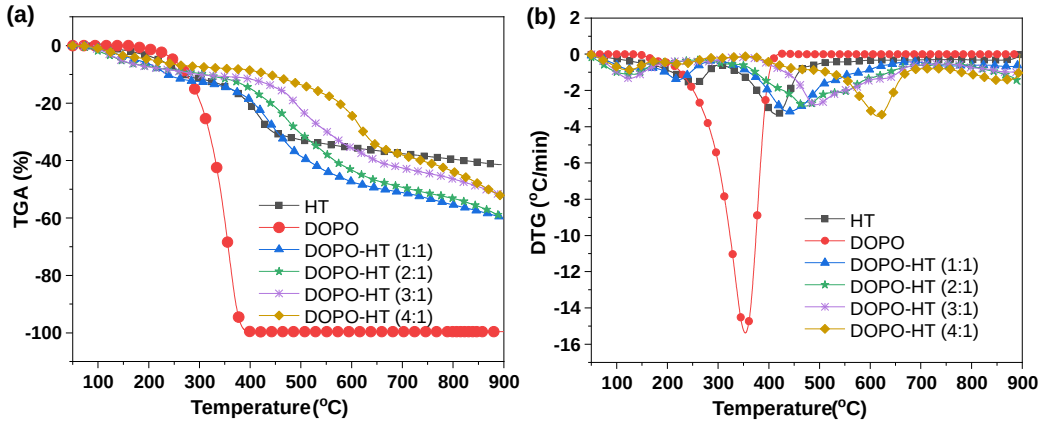


Figure 3.20. TGA (a) and DTG (b) curves of nHT, DOPO, and DOPO-HT samples with different DOPO:HT ratios under a nitrogen ($N_2$) atmosphere

From the TGA and DTG analyses (Figure 3.20) revealed that pristine hydrotalcite undergoes two degradation stages, while DOPO exhibits poor thermal stability with negligible char formation. After modification, DOPO–HT samples showed decreased $T_{max1}$, increased $T_{max2}$, and significantly enhanced char yield at 900 °C. In particular, $HT_3$ (DOPO:HT = 3:1) achieved the highest residue (~47.78%), evidencing a strong synergistic interaction between the organic and inorganic phases.

The thermal analysis results revealed that the DOPO-HT compounds exhibited different thermal stabilization behaviors depending on the type of hydrotalcite employed. The initial heating stage was associated with the loss of physically adsorbed water and the decomposition of hydroxyl groups, whereas XRD analysis after calcination at 900 °C indicated that $HT_1$ and $HT_2$ formed $Mg_3(PO_4)_2$, while $HT_3$ and $HT_4$ yielded $Mg_2P_2O_7$. The latter phase demonstrated superior thermal protection capability, which accounts for the higher residual char content and highlights the crucial role of the initial structural configuration in determining the thermal resistance and flame-retardant performance of DOPO-HT.

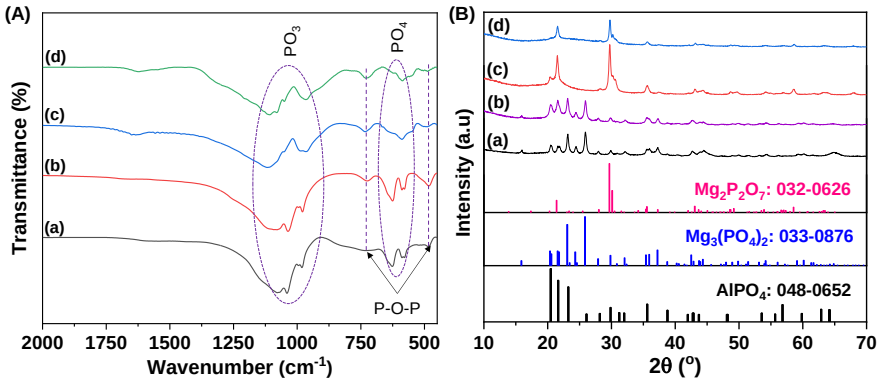


Figure 3.21. FT-IR spectra (A) and XRD patterns (B) of $HT_1$ (a), $HT_2$ (b), $HT_3$ (c), and $HT_4$ (d) samples after calcination at 900 °C

*+ Dispersion capability of modified HT in the epoxy matrix*

The dispersion behavior of DOPO-modified HT within the EP matrix was evaluated by XRD and SEM-EDX. The XRD results revealed that all samples from 3HT/7IFR/EP to $3HT_4$/7IFR/EP retained the characteristic peaks of APP; however, only samples from $3HT_2$/7IFR/EP onwards exhibited weak or vanished HT peaks, indicating effective intercalation and exfoliation due to the highly disordered structure and the P–H interaction (DOPO) with EP. Complementary SEM-EDX analysis showed that Mg and Al were heterogeneously distributed in 3HT/7IFR/EP but became uniformly dispersed in $3HT_3$/7IFR/EP, thereby confirming the superior dispersion of $HT_3$ within the EP matrix.

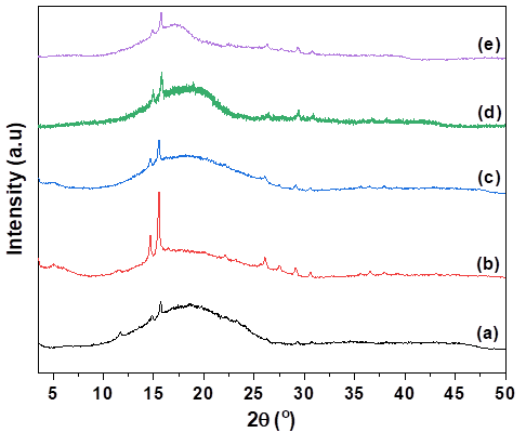


Figure 3.22. XRD patterns of the nanocomposite samples 3HT/7IFR/EP (a), $3HT_1$/7IFR/EP (b), $3HT_2$/7IFR/EP (c), $3HT_3$/7IFR/EP (d), and $3HT_4$/7IFR/EP (e)

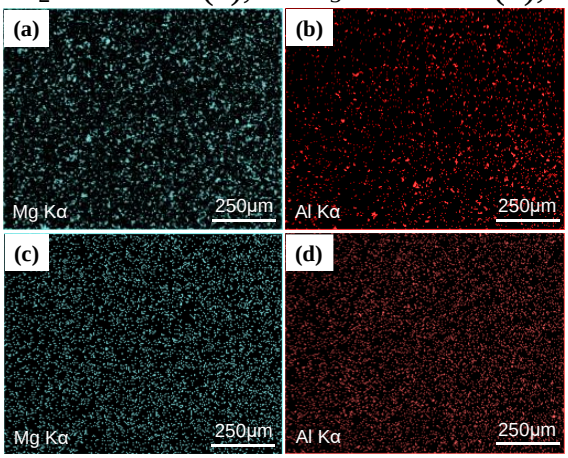


Figure 3.23. EDX elemental mapping of Mg and Al in the nanocomposite samples 3HT/7IFR/EP (a, b) and $3HT_3$/7IFR/EP (c, d)

## 3.2. Results of the study on the fabrication of flame-retardant polymer nanocomposites

### *3.2.1. Results of the study on the fabrication of flame-retardant polypropylene-based composites containing nano zinc borate*

*3.2.1.1. Flame-retardant properties of polypropylene-based composites containing nano zinc borate additives*

Table 3.3. Flame-retardant and mechanical properties of PP and its composites

| Sample | UL94-V rating | LOI (%) | Tensile strength (MPa) | Elongation (%) | Impact strength ($kJ/m^2$) |
|---|---|---|---|---|---|
| Neat PP | No rating | 16.8 | 25.84 ± 0.6 | 62.93 ± 8.0 | 60.46 ± 5.3 |
| 21ZB/PP | No rating | 19.3 | 24.67 ± 0.2 | 40.49 ± 5.0 | 37.55 ± 3.3 |
| 21RP/PP | No rating | 21.1 | 23.55 ± 0.5 | 38.18 ± 6.0 | 22.64 ± 2.0 |
| 21EG/PP | No rating | 20.2 | 22.02 ± 1.0 | 19.07 ± 5.0 | 11.27 ± 1.0 |
| 21n-ZB/PP | No rating | 19.7 | 25.17 ± 0.2 | 58.85 ± 4.0 | 40.25 ± 3.5 |
| 7ZB/7RP/7EG/PP | V-1 | 23.2 | 23.69 ± 0.7 | 30.17 ± 6.0 | 24.68 ± 2.2 |
| 7n-ZB/7RP/7EG/PP | V-1 | 23.7 | 24.62 ± 0.4 | 35.12 ± 5.0 | 28.15 ± 2.5 |

The flame-retardant performance of PP and its composites is summarized in Table 3.3. The individual incorporation of ZB, RP, or EG (21 wt%) only increased the LOI value from 16.8% to 19.3–21.1%, without achieving a UL94-V rating. In contrast, the ternary system (7ZB/7RP/7EG/PP) achieved a UL94 V-1 classification with an LOI of 23.2%. Furthermore, replacing ZB with nano-sized ZB (7n-ZB/7RP/7EG/PP) further improved the LOI to 23.7%.

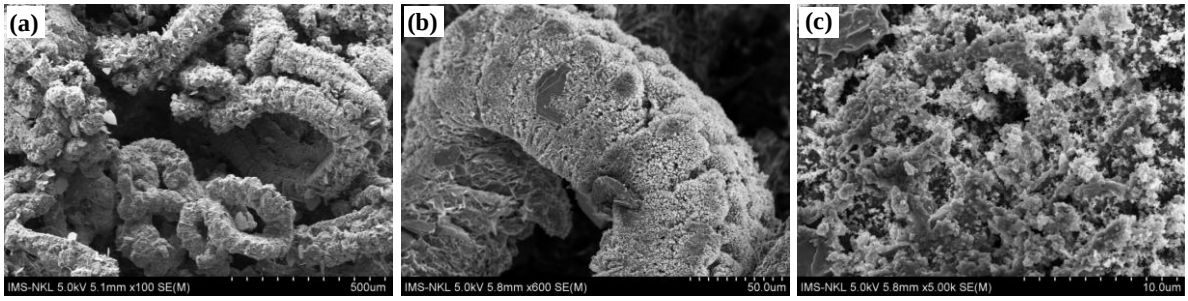


Figure 3.24. SEM images of the 7n-ZB/7RP/7EG/PP composite after the UL94-V flammability test at different magnifications

SEM (Figure 3.24) observations revealed a clear synergistic effect: the expansion of EG generated a protective char layer; RP decomposed to form a phosphorus oxide barrier; the release of water from ZB promoted acid-catalyzed charring; and the thermal decomposition of ZB yielded a zinc phosphate–silicate glassy layer. These combined mechanisms enhanced char strength and effectively suppressed polymer dripping.

*3.2.1.2. Thermal behavior of polypropylene-based composites incorporating nano zinc borate*

TGA analysis in air indicated that neat PP undergoes complete decomposition at 510 °C, with $T_{5\%}$ = 320.6 °C, $T_{max}$ = 431.9 °C, and a residual char yield of 0.1%. In contrast, the 7n-ZB/7RP/7EG/PP nanocomposite exhibits a

lower $T_{5\%}$ due to the early dehydration of zinc borate (~180 °C), whereas its Tmax increases to 445.7 °C and the residual char yield reaches 14.67%. These findings demonstrate the flame-retardant role of the additive system in facilitating the formation of a thermally insulating barrier layer, thereby suppressing heat transfer and improving the thermal stability of PP.

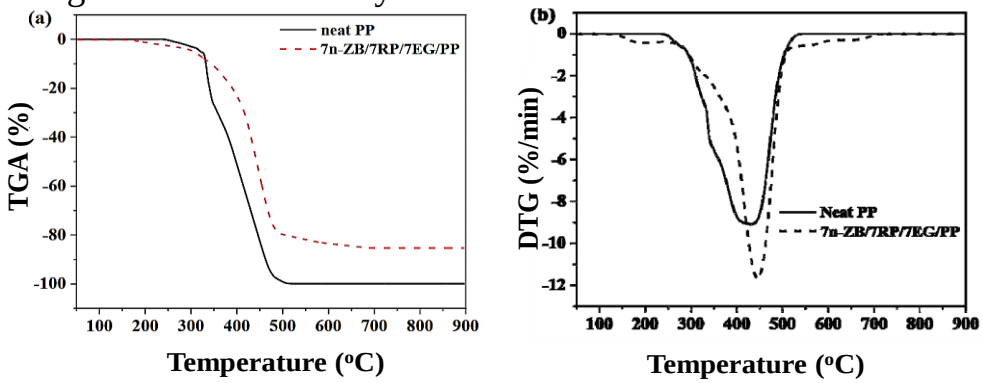


Figure 3.25. TGA (a) and DTG (b) curves of neat PP and the 7n-ZB/7RP/7EG/PP composite in air

Table 3.4. Thermogravimetric analysis data of neat PP and the 7n-ZB/7RP/7EG/PP nanocomposite in air

| sample | $T_{5\%}$ (°C) | $T_{max}$ (°C) | Residue at 900 °C (Wt.%) |
|---|---|---|---|
| Neat PP | 320.6 | 431.9 | 0.1 |
| 7n-ZB/7RP/7EG/PP | 296.5 | 445.7 | 14.67 |

XRD analysis of the 7n-ZB/7RP/7EG/PP nanocomposite calcined at 900 °C (Figure 3.26) reveals that, prior to calcination, characteristic diffraction peaks of PP (14.18°, 16.87°, 18.71°, 21.27°, 22.10°), EG (26.64°, 54.75°), and ZB are observed. After calcination, the formation of $B(OH)_3$, $Zn_4O(BO_2)_6$, and $Zn_3(PO_4)_2$ is detected as a result of interactions between ZB and RP, while the diffraction peaks of EG remain. This transformation accounts for the enhanced flame retardancy and thermal stability, consistent with the high residual char content obtained from TGA analysis.

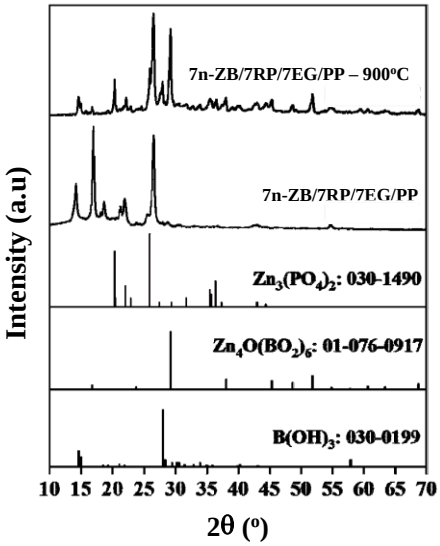


Figure 3.26. XRD patterns of the 7n-ZB/7RP/7EG/PP composite before and after calcination at 900 °C

*3.2.1.3. Mechanical properties of polypropylene-based composites incorporating nano zinc borate*

The mechanical properties results (Table 3.3, Figure 3.27) show that the incorporation of flame-retardant additives reduces the tensile strength, elongation at break, and impact strength of PP, with EG causing the most pronounced deterioratio (the 21EG/PP sample exhibits decreases of 14.78%, 69.70%, and 81.36%, respectively), due to its poor interfacial interaction with the polymer matrix and the large particle size that induces structural defects (Figure 3.28). In contrast, replacing micrometer-sized ZB with nZB significantly improves the mechanical performance; the 7n-ZB/7RP/7EG/PP composite achieves a tensile strength of 24.62 MPa and an elongation at break of 35.12%, attributed to the improved dispersion of nano zinc borate within the polymer matrix.

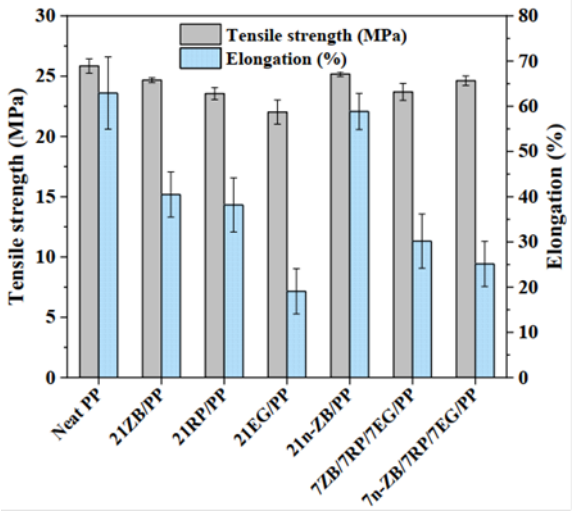


Figure 3.27. Mechanical properties of neat PP and its composites

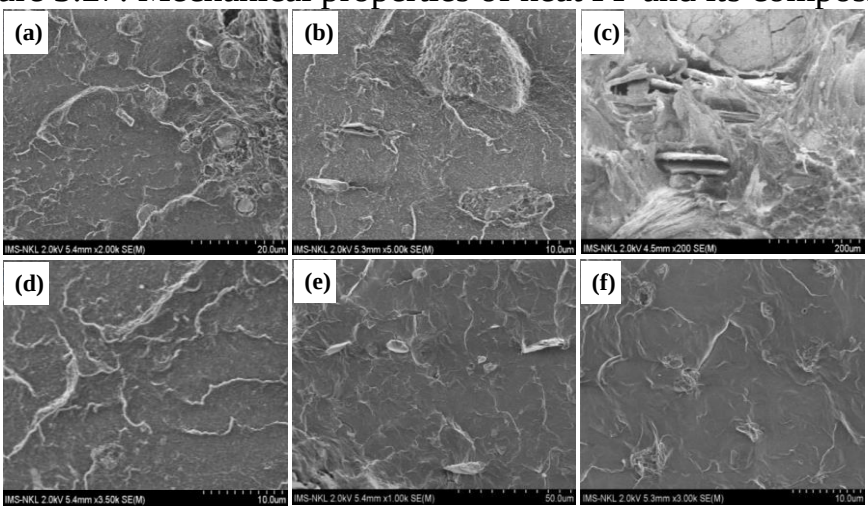


Figure 3.28. SEM images of the fracture surfaces of PP-based composite samples after tensile testing: 21ZB/PP (a), 21RP/PP (b), 21EG/PP (c), 21n-ZB/PP (d), 7ZB/7RP/7EG/PP (e), and 7n-ZB/7RP/7EG/PP (f)

***3.2.2. Results of the study on the fabrication of flame-retardant epoxy resin–based composites incorporating nano aluminum hydroxide***

*3.2.2.1. Flame-retardant properties of epoxy resin–based composites incorporating nano aluminum hydroxide*

The UL94-V and LOI test results (Table 3.5) indicate that neat EP is highly flammable (LOI = 21.1%), whereas the 10APP@PEI/EP sample achieves a V-0

rating and an LOI of 28.9%. Replacing part of APP@PEI with $nATH_{PEI}$ further increases the LOI to 31.1% and shortens the after-flame times ($t_1$ = 0.6 s, $t_2$ = 0.8 s) at loadings ≤ 3%, due to improved dispersion and synergistic effects. However, at higher $nATH_{PEI}$ contents, the flame-retardant performance deteriorates; for instance, the $5nATH_{PEI}$/5IFR/EP sample only reaches a V-1 rating with an LOI of 28.1%. These results suggest that the optimal $nATH_{PEI}$ content is 3%.

Table 3.5. Flame-retardant performance and mechanical properties of EP resin and its composites containing nATH

| No. | Samples | UL94-V (3.2 mm) | | | LOI (%) | Tensile strength (MPa) | Impact strength ($KJ/m^2$) |
|---|---|---|---|---|---|---|---|
| | | Rating | $t_1$[a] (s) | $t_2$[b] (s) | | | |
| 1 | EP | NR* | Burnt out | - | 21.1 | 83.69 ± 0.2 | 45.92 ± 0.1 |
| 2 | 10APP@PEI/EP | V-0 | 3.3 | 5.8 | 28.9 | 59.84 ± 0.6 | 12.57 ± 0.3 |
| 3 | 3ATH/7IFR/EP | V-1 | 0.9 | 13.6 | 28.5 | 58.82 ± 0.7 | 14.54 ± 0.6 |
| 4 | $3ATH_{OA}$/7IFR/EP | V-0 | 1.0 | 2.5 | 30.7 | 66.15 ± 0.3 | 21.54 ± 0.2 |
| 5 | $3ATH_{Tw80}$/7IFR/EP | V-0 | 0.8 | 3.2 | 29.4 | 64.22 ± 0.5 | 19.83 ± 0.5 |
| 6 | $3ATH_{PEI}$/7IFR/EP | V-0 | 0.6 | 0.8 | 31.1 | 67.80 ± 0.2 | 22.68 ± 0.1 |
| 7 | $1ATH_{PEI}$/9IFR/EP | V-0 | 3.4 | 2.6 | 29.8 | 62.89 ± 0.1 | 20.15 ± 0.2 |
| 8 | $5ATH_{PEI}$/5IFR/EP | V-1 | 3.1 | 15.4 | 28.1 | 68.44 ± 0.5 | 23.46 ± 0.4 |
| 9 | $10ATH_{PEI}$/EP | NR | Burnt out | - | 22.8 | 71.65 ± 0.4 | 29.70 ± 0.3 |

* *NR: No rating*

[a]$t_1$*: After-flame time following the first ignition;* [b]$t_2$*: After-flame time following the second ignition*

*3.2.2.2. Thermal behavior of epoxy resin–based composites incorporating nano aluminum hydroxide*

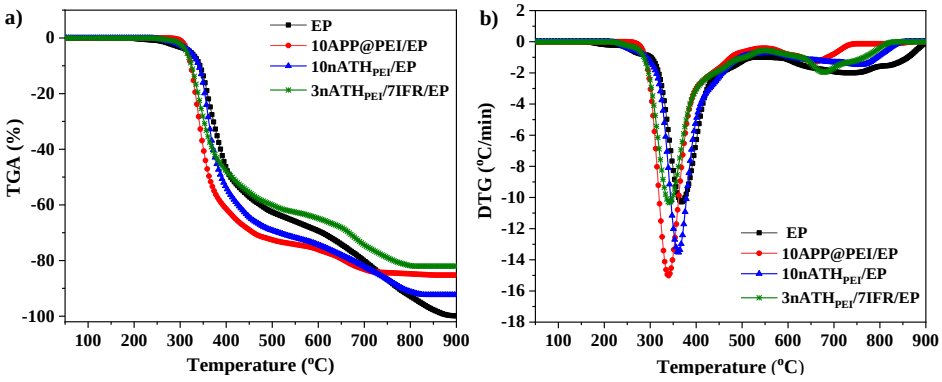


Figure 3.29. TGA (a) and DTG (b) curves of neat EP and its composite samples in an air atmosphere

TGA/DTG analyses (Figure 3.29, Table 3.6) show that neat epoxy (EP) undergoes a two-step decomposition, leaving only 0.12% residue at 900 °C. In contrast, the 10APP@PEI/EP sample yields 14.75% char as a result of carbonization induced by APP decomposition products. The $10nATH_{PEI}$/EP sample exhibits an increase in $T_{max_2}$ by 40.28 °C and produces 7.62% char,

indicating that $nATH_{PEI}$ enhances thermo-oxidative stability. Moreover, the $3nATH_{PEI}$/7IFR/EP sample achieves the highest char yield (17.98%) and shows an increase in $T_{max_2}$ by 20.61 °C compared to 10APP@PEI/EP, reflecting the synergistic effect of APP@PEI and $nATH_{PEI}$ through the formation of thermally stable aluminum phosphate.

Table 3.6. Thermogravimetric analysis data of EP resin and its composites containing nATH in air

| Samples | $T_{5\%}$ [a] (°C) | $T_{max1}$ [b] (°C) | $T_{max2}$ [c] (°C) | Residue at 900°C (%) |
|---|---|---|---|---|
| EP | 317.54 | 368.31 | 714.15 | 0.12 |
| 10APP@PEI/EP | 316.24 | 339.72 | 659,15 | 14.75 |
| $10ATH_{PEI}$/EP | 322.2 | 361.12 | 764.43 | 7.62 |
| $3ATH_{PEI}$/7IFR/EP | 314.21 | 341.65 | 679.76 | 17.98 |

[a] *$T_{5\%}$: Temperature at 5% weight loss;*

[b, c] *$T_{max}$: Temperature corresponding to the maximum decomposition rate.*

*3.2.2.3. Flame-retardant mechanism of epoxy resin–based composites incorporating nano aluminum hydroxide*

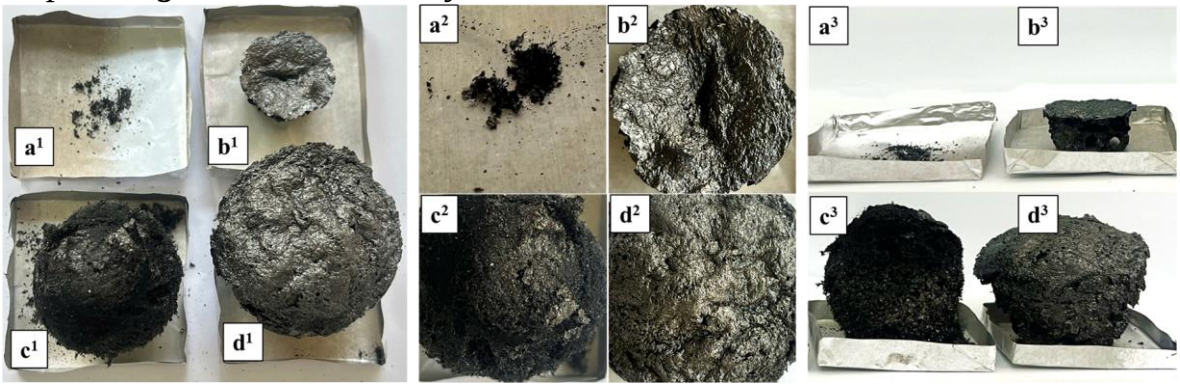


Figure 3.30. Char structural images of EP and its composites after calcination at 900°C: EP (a), $10nATH_{PEI}$/EP (b), 10APP@PEI/EP (c), and $3nATH_{PEI}$/7IFR/EP (d)

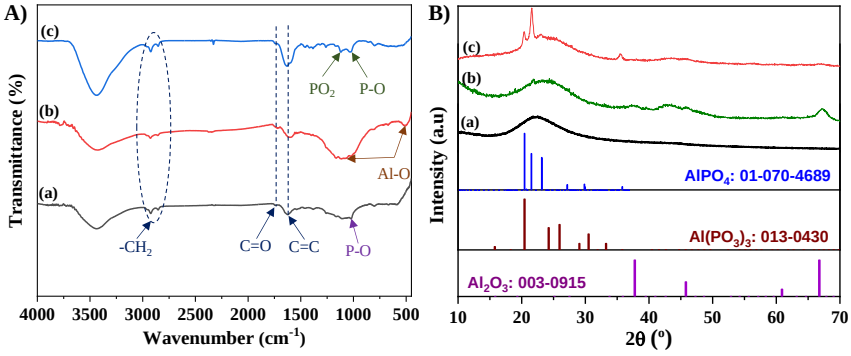


Figure 3.31. FT-IR spectra (A) and XRD patterns (B) of the char residues of the composite samples: 10APP@PEI/EP (a), $10ATH_{PEI}$/EP (b), and $3ATH_{PEI}$/7IFR/EP (c) after combustion at 900 °C

Based on char observation (Figure 3.30), FT-IR analysis (Figure 3.31A), XRD patterns (Figure 3.31B), and SEM-EDX results (Figure 3.32), the flame-retardant mechanism of epoxy resin–based composites incorporating nATH is proposed as follows. APP@PEI decomposes to generate phosphoric acid and

$NH_3/H_2O$, which dilute combustible species, while nATH decomposes to produce $H_2O$ and $Al_2O_3$, which reacts with the decomposition products of APP to form thermally stable $AlPO_4$, reinforcing the char layer.

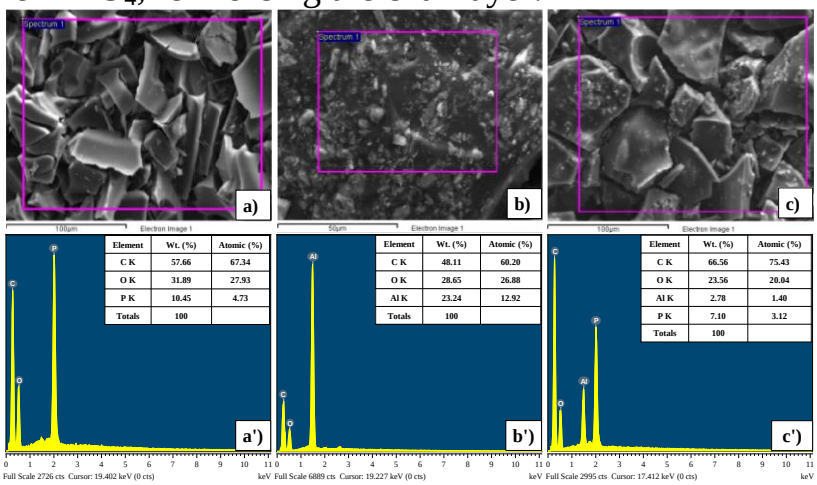


Figure 3.32. SEM images and EDX spectra of the char residues of 10APP@PEI/EP (a, a'), $10ATH_{PEI}$/EP (b, b'), and $3ATH_{PEI}$/7IFR/EP (c, c') after combustion at 900 °C

As a result, the char layer of the $3nATH_{PEI}$/7IFR/EP composite is dense, continuous, and durable, providing an effective condensed-phase flame-retardant mechanism. This structure acts as a barrier to heat and mass transfer, thereby enhancing flame retardancy. The proposed mechanism is illustrated in Figure 3.33.

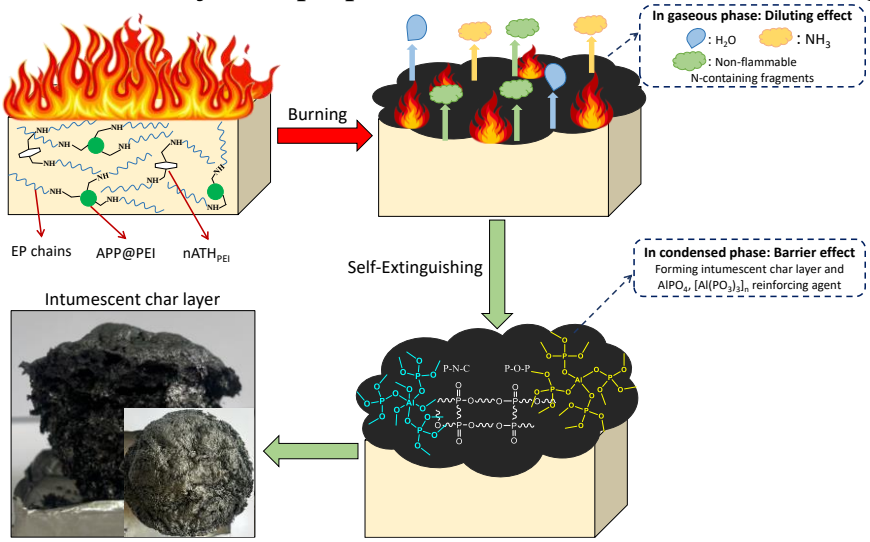


Figure 3.33. Schematic illustration of the flame-retardant mechanism of the $3nATH_{PEI}$/7IFR/EP nanocomposite

*3.2.2.4. Mechanical properties of epoxy resin–based composites incorporating nano aluminum hydroxide*

The incorporation of APP@PEI alone significantly deteriorates the mechanical performance of epoxy resin (Table 3.5). In contrast, partial replacement with untreated nATH does not lead to improvement, due to agglomeration, defect formation, and poor interfacial compatibility with the polymer matrix (SEM images, Figure 3.34). On the other hand, $nATH_{PEI}$ imparts a remarkable reinforcing effect: the $3nATH_{PEI}$/7IFR/EP system exhibits tensile strength and impact strength enhancements of 13.30% and 80.43%, respectively, compared with 10APP@PEI/EP, owing to uniform dispersion and strong interfacial adhesion. These findings demonstrate that the mechanical properties of the nanocomposites increase with the

content of $nATH_{PEI}$, with the composition of 3 wt% $nATH_{PEI}$ and 7 wt% APP@PEI being optimal, simultaneously ensuring flame retardancy and superior mechanical performance.

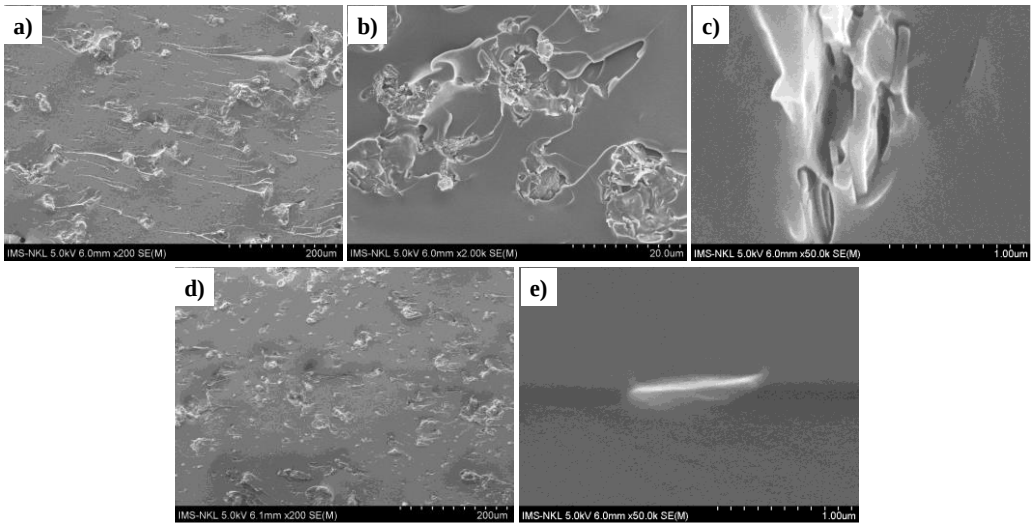


Figure 3.34. SEM images of the fracture surfaces of EP nanocomposite samples after tensile testing: 3nATH/7IFR/EP (a, b, c) and 3$nATH_{PEI}$/7IFR/EP (d, e)

***3.2.3. Results of the study on the fabrication of flame-retardant epoxy resin–based composites incorporating nano hydrotalcite***

*3.2.3.1. Flame-retardant properties of epoxy resin–based composites incorporating nano hydrotalcite*

The flame retardancy of epoxy nanocomposites was evaluated using UL-94 and LOI tests, and the results are summarized in Table 3.7. Incorporating 10 wt% APP@PEI increased the LOI value from 21.1% to 28.9% and achieved a V-0 rating, while replacing 3 wt% with unmodified nHT reduced the UL-94 rating to V-1 and the LOI to 25.9% due to particle agglomeration.

Table 3.7. Flame-retardant performance and mechanical properties of EP resin and its composites containing nHT

| No. | Sample | UL94-V (3.2 mm) | | | LOI (%) | Tensile strength (MPa) | Impact strength ($KJ/m^2$) |
|---|---|---|---|---|---|---|---|
| | | Rating | $t_1^a$ (s) | $t_2^b$ (s) | | | |
| 1 | EP | NR | Burnt out | - | 21.1 | 83.69 ± 0.2 | 45.92 ± 0.1 |
| 2 | 10APP@PEI/EP | V-0 | 3.3 | 5.8 | 28.9 | 59.84 ± 0.6 | 12.57 ± 0.3 |
| 3 | 3HT/7IFR*/EP | V-1 | 1.5 | 14.3 | 25.9 | 62.53 ± 0.3 | 12.62 ± 0.5 |
| 4 | $3HT_1$/7IFR/EP | V-0 | 0.8 | 8.9 | 27.6 | 63.08 ± 0.5 | 18.48 ± 0.2 |
| 5 | $3HT_2$/7IFR/EP | V-0 | 1.0 | 3.3 | 30.7 | 66.22 ± 0.1 | 21.65 ± 0.3 |
| 6 | $3HT_3$/7IFR/EP | V-0 | 0.7 | 0.5 | 32 | 68.83 ± 0.2 | 22.58 ± 0.1 |
| 7 | $3HT_4$/7IFR/EP | V-0 | 0.9 | 1.7 | 30.7 | 65.36 ± 0.7 | 19.86 ± 0.4 |

*$t_1^a$: Self-extinguishing time after the first ignition; $t_2^b$: Self-extinguishing time after the second ignition; *IFR: APP@PEI*

*3.2.3.2. Thermal behavior of epoxy resin–based composites incorporating nano hydrotalcite*

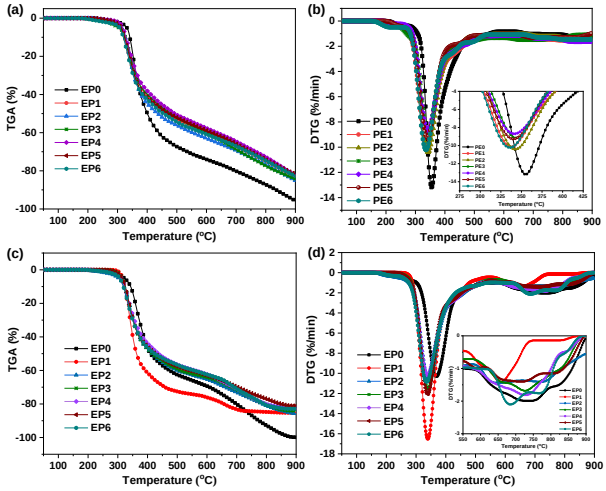


Figure 3.35. TGA and DTG curves of EP and its composites under $N_2$ (a, b, and inset) and air (c, d, and inset) atmosphere

*EP1: 10APP@PEI/EP; EP2: 3HT/7IFR/EP; EP3: $3HT_1$/7IFR/EP; EP4: $3HT_2$/7IFR/EP; EP5: $3HT_3$/7IFR/EP; EP6: $3HT_4$/7IFR/EP

Table 3.8. Thermogravimetric analysis data of EP resin and its composites containing nHT

| Sample | $N_2$ | | | Air | | | |
|---|---|---|---|---|---|---|---|
| | $T_{5\%}$ [a] (°C) | $T_{max}$ [b] (°C) | Residue (%) | $T_{5\%}$ (°C) | $T_{max}$ (°C) | | Residue (%) |
| | | | | | 1 | 2 | |
| EP | 331.52 | 354.95 | 3.2 | 317.54 | 368.31 | 718.45 | 0.12 |
| 10APP@PEI/EP | 309.95 | 337.37 | 15.82 | 316.24 | 339.72 | 657.85 | 14.75 |
| 3HT/7IFR/EP | 313.38 | 342.41 | 13.71 | 304.44 | 342.82 | 781.21 | 13.57 |
| $3HT_1$/7IFR/EP | 304.72 | 341.12 | 14.83 | 315.32 | 339.93 | 728.67 | 15.75 |
| $3HT_2$/7IFR/EP | 317.67 | 343.01 | 16.22 | 312.21 | 337.92 | 727.72 | 17.60 |
| $3HT_3$/7IFR/EP | 312.01 | 339.98 | 17.53 | 314.77 | 339.12 | 724.80 | 18.90 |
| $3HT_4$/7IFR/EP | 306.85 | 335.83 | 15.90 | 306.85 | 335.21 | 679.14 | 17.12 |

[a] *$T_{5\%}$: Temperature at 5% weight loss;*

[b] *$T_{max}$: Temperature corresponding to the maximum decomposition rate.*

According to the thermogravimetric results (Figure 3.35 and Table 3.8), the epoxy nanocomposites containing HT combined with APP@PEI began to decompose at lower temperatures than neat EP, indicating that the flame retardant promoted dehydration and carbonization, thus facilitating the formation of a stable char layer. The reduced maximum decomposition rate and increased char yield confirmed the positive effect of the flame retardant on thermal stability. In air, the composites showed better oxidation resistance, with $3HT_3$/7IFR/EP exhibiting the highest char residue (17.53% at 900 °C), demonstrating that HT-DOPO significantly enhanced the thermal stability and flame retardancy of the EP matrix.

*3.2.3.3. Flame-retardant mechanism of epoxy resin–based composites incorporating nano hydrotalcite*

Analysis of the residual char by SEM, FT-IR, XRD, and EDX (Figures 3.36–3.39) revealed that the incorporation of the DOPO-HT nanohybrid in combination

with APP@PEI significantly improved the formation of a continuous, compact, and phosphorus-rich char layer, instead of the porous and brittle char observed in 10APP@PEI/EP. The 3HT$_3$/7IFR/EP sample exhibited a synergistic interaction between DOPO-HT and APP@PEI, which resulted in a stable intumescent char structure containing P–N–C networks, polyphosphates, and metal phosphates, thereby reinforcing thermal stability.

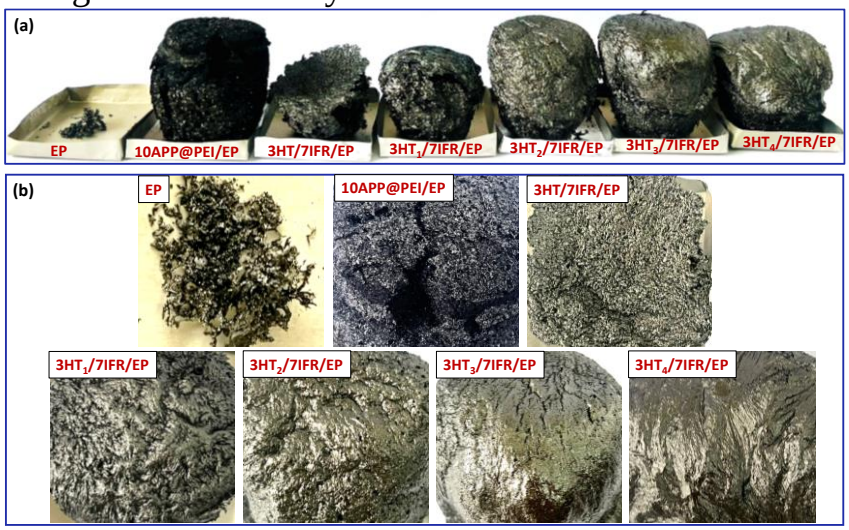


Figure 3.36. Photographic images of the char layers of EP and its composites after combustion at 900 $^o$C: Side view (a) and Top view (b)

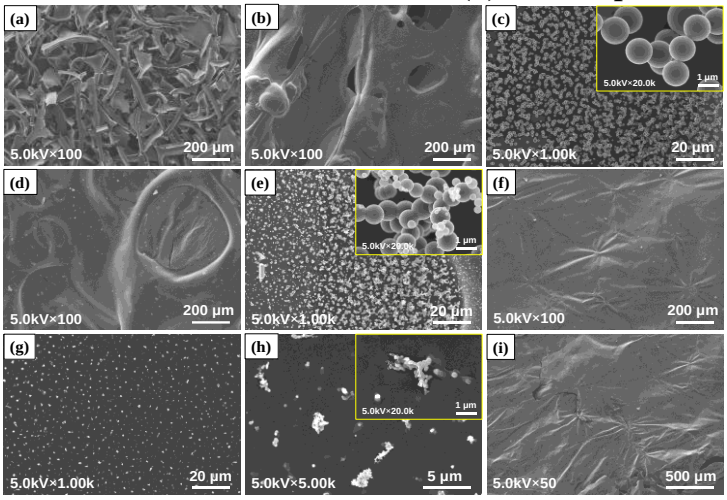


Figure 3.37. SEM images of the sample surfaces: 10APP@PEI/EP (a), 3HT$_1$/7IFR/EP (b, c), 3HT$_2$/7IFR/EP (d, e), 3HT$_3$/7IFR/EP (f–h) và 3HT$_4$/7IFR/EP (i) aftercalcination at 900 $^o$C

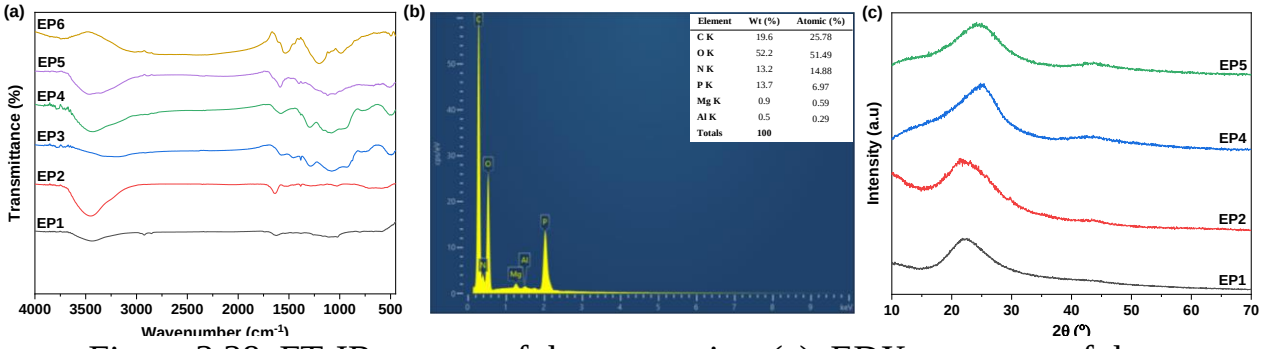


Figure 3.38. FT-IR spectra of the composites (a), EDX spectrum of the 3HT$_3$/7IFR/EP sample (b), and XRD patterns of the composites (c) after calcination at 900 $^o$C

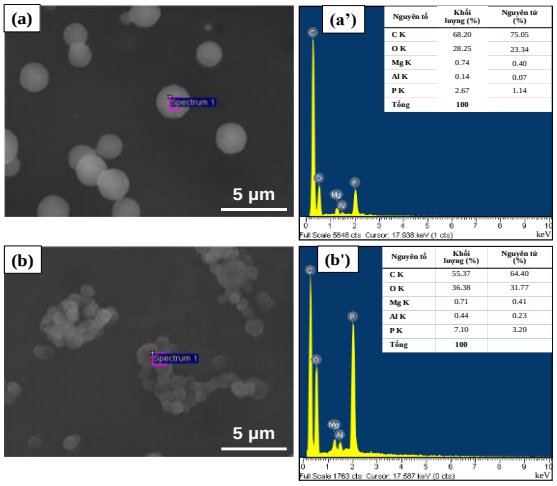


Figure 3.39. EDX analysis results of the spherical particles on the surface of the char residue of the $3HT_1$/7IFR/EP (a, a') and $3HT_3$/7IFR/EP (b, b') samples

The proposed flame-retardant mechanism (Figure 3.40) consists of both gas-phase actions (radical scavenging and release of non-flammable gases) and condensed-phase actions (formation of a robust phosphorus-rich char layer), markedly enhancing the flame retardancy of the epoxy nanocomposites.

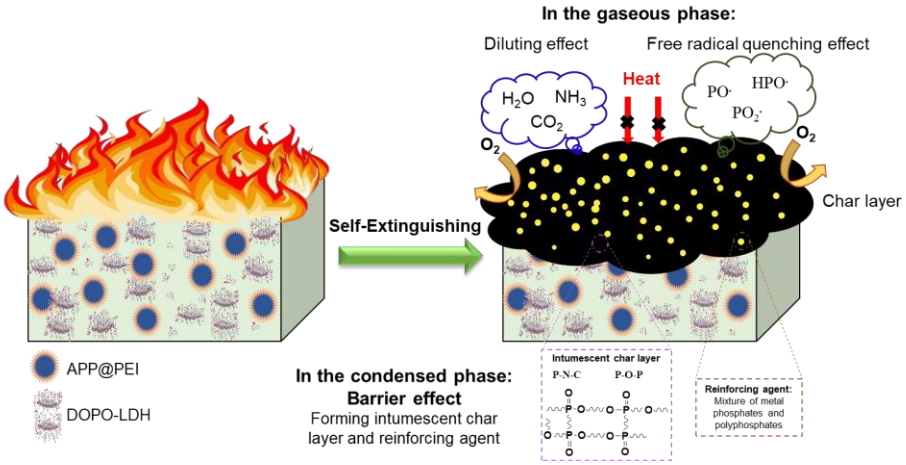


Figure 3.40. Schematic illustration of the flame-retardant mechanism of the epoxy nanocomposite containing APP@PEI and DOPO-HT nanohybrids

*3.2.3.4. Mechanical properties of epoxy resin–based composites incorporating nano hydrotalcite*

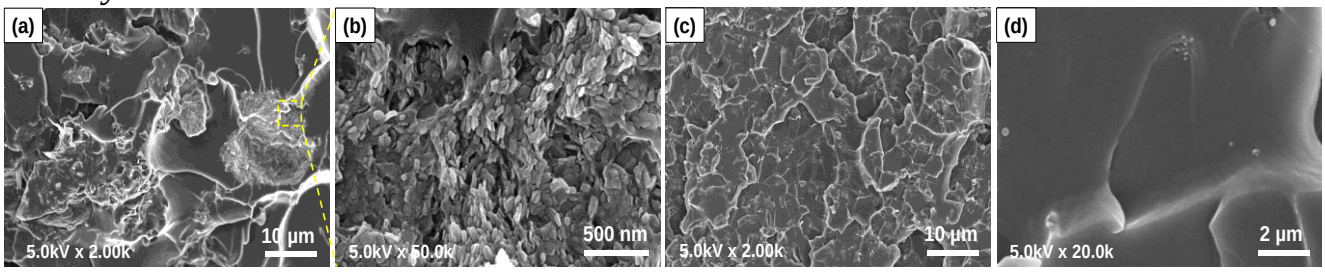


Figure 3.41. SEM images of the fracture surfaces of EP nanocomposite samples after tensile testing: 3HT/7IFR/EP (a, b) and $3HT_3$/7IFR/EP (c, d)

The mechanical test results (Table 3.7) show that adding APP@PEI decreases the tensile and impact strengths due to particle agglomeration and poor interfacial compatibility (Figures 3.41a, b). Partial substitution with unmodified HT yields only slight improvement, as agglomeration remains (Figures 3.23a, b; 3.41a, b). In contrast, DOPO-modified HT significantly enhances mechanical

performance, particularly at a DOPO:HT ratio of 3:1, owing to its better dispersion in the EP matrix (Figures 3.22d; 3.23c, d; 3.41c, d). However, further increasing the ratio to 4:1 slightly reduces performance, likely due to fewer reinforcing particles and DOPO interference with EP curing. Therefore, the 3:1 ratio is considered optimal for the DOPO-modified HT nanocomposite.

## CONCLUSIONS AND RECOMMENDATIONS

### 1. Conclusions

- nZB ($2ZnO.3B_2O_3.3H_2O$) was successfully synthesized via a precipitation method using oleic acid as a surfactant; the particles are thin platelets with diameters of 1.0 - 1.5 μm, thickness of ~90 nm, hydrophobic, and well compatible with PP.

- nATH was successfully synthesized by a hydrothermal method; the particles are hexagonal platelets with diameters of 200 - 300 nm and thickness of ~50 nm, and after surface modification with PEI, they are uniformly dispersed in EP.

- nHT was synthesized via co-precipitation; uniform platelets, 150 - 200 nm in diameter, ~20 nm thick, and after DOPO hybridization, show good compatibility and dispersion in EP.

-Flame-retardant PP-based composites were successfully fabricated. The combination of nZB, RP, and EG exhibited a pronounced synergistic flame-retardant effect. The 7nZB/7RP/7EG/PP sample achieved a UL-94 V-1 rating, an LOI value of 23.7%, and showed a significant reduction in mechanical deterioration compared with neat PP.

- Flame-retardant EP-based composites were successfully developed. The synergistic incorporation of $nATH_{PEI}$ or DOPO-HT with APP@PEI produced a strong synergistic effect. The representative samples $3nATH_{PEI}$/7IFR/EP and $3HT_3$/7IFR/EP achieved UL-94 V-0 classification and LOI values above 30%, while significantly reducing the deterioration of mechanical properties compared with the neat resin. The flame-retardant mechanism was proposed based on the synergistic interactions among the additives in the EP-based composites.

### 2. Recommendations

Based on the achieved results, the dissertation demonstrated the effectiveness and application potential of inorganic nano materials such as nZB, nATH, and nHT in the fabrication of flame-retardant polymer nanocomposites, particularly when surface-modified or hybridized with halogen-free organic compounds. The inorganic nano additives played a crucial role in enhancing the flame retardancy, thermal stability, and mechanical performance of the composites, while offering a promising pathway toward high-performance and environmentally friendly inorganic–organic hybrid systems. Future studies should focus on optimizing synthesis and modification processes, improving dispersion, and extending the approach to other polymer matrices to further advance the practical application of flame-retardant polymer composites incorporating inorganic nano additives.

## SCIENTIFIC PUBLICATION

[1]. Cong Doanh Truong, Thi Nhung Hac, Thi Hanh Nguyen, Thi Thu Hien Nguyen, Tien Dat Doan, Minh Tan Vu, Mai Ha Hoang, (2022), "Synthesis of Nanoplatelet Zinc Borate and its Combination with Expandable Graphite and Red Phosphorus as Flame Retardants for Polypropylene", VNU Journal of Science: Natural Sciences and Technology, Vol. 38 (No. 3), pp. 86-96, https://doi.org/10.25073/2588-1140/vnunst.5402.

[2]. Truong Cong Doanh, Nhung Hac Thi, Hong Tham Nguyen, Ho Thi Oanh, Tien Dat Doan, Nguyen Duc Tuyen, Minh-Tan Vu, Mai Ha Hoang (2025), "Preparation and synergistic effect of aluminum hydroxide nanoplates on the fire resistance and thermal stability of the intumescent flame retardant epoxy composite", RSC Advances, Vol. 15, pp. 16814–16825, https://doi.org/10.1039/D5RA00231A.

[3]. Nguyen Hong Tham, Nhung Hac Thi, Truong Cong Doanh, Tran Duc Long, Ho Thi Oanh, Tien Dat Doan, Nguyen Duc Tuy, Minh-Tan Vu, Mai Ha Hoang (2025), "Enhancement in the fire resistant efficiency of epoxy resin by synergistic effect between metal-organic frameworks and polyethyleneimine-modified ammonium polyphosphate", Hanoi University of Industry Journal of Science and Technology, Vol. 61 (No. 7V), pp. 170-180, 7/2025, http://doi.org/10.57001/huih5804.2025.298.

[4]. Nhung Hac Thi, Truong Cong Doanh, Hong Tham Nguyen, Ho Thi Oanh, Tien Dat Doan, Mai Ha Hoang (2025), "DOPO-Intercalated Layered Double Hydroxide: A Synergistic Flame-Retardant Nanohybrid for High Performance Epoxy Composite", Journal of Applied Polymer Science, Vol. 0, e57993, https://doi.org/10.1002/app.57993.